Tools and Strategies for 3D EM Modeling and Design of Microwave Imaging Systems for Medical Applications

1. Introduction

Microwave Imaging (MWI) has attracted massive attention in the medical research field over the last decade due to its standout qualities of utilizing harmless non-ionizing radiation and affordable components. At present, the conventional technologies such as Computed Tomography (CT) and Magnetic Resonance Imaging (MRI), which provide high resolution images, still have several limitations such as their long examination time, non-portability, high cost and also the ionizing radiation.

MWI has several potential applications and one of the promising areas is malignant tissue detection as a contrast of permittivity with respect to healthy tissues inside the human body. These unhealthy tissues have possibility of becoming benign or malicious tumor or stroke and are prone to increase the size of the healthy lymph nodes to more than 1 cm (considered to be malicious) over the time inside the head, breast, axilla or abdominal area. In order to detect malignancy using MWI at different organs, particular imaging scenarios need to be considered.

An indispensable tool for the design, testing, and functioning of medical devices, which are based on microwave imaging algorithms, is a powerful 3D EM simulation environment [1]. In this work we propose such an environment built around WIPL-D Pro, as an efficient and flexible general purpose 3D EM solver [2,3]. In addition, libraries of phantoms and appropriate antennas are developed, as well as tools and strategies to create the library components and MWI scenarios [4,5].

These features can be understood from step-by-step demonstration of development stages of a 3D Model of NEVA head with the 21-antenna system, the scenario created in a line of Refs. [6,7]. Accuracy and usability of 3D EM simulation is shown using results for s-parameters and near-field for scenarios with and without stroke. Finally, it was demonstrated that by post-processing these results using TSVD (Truncated Singular Value Decomposition) method the position and size of the stroke can be successfully detected [8].

Creation of head phantom model starting from STL (triangle based) files of human body is explained in Chapter 2. Near field results with and without stroke for plane wave excitation are given in Chapter 3. Adjustments to an antenna, chosen from the antenna library and used with the head phantom model are described in Chapter 4. Semi-automatic design of antenna array helmet is demonstrated in Chapter 5. Accuracy and usability of the scenario with and without stroke for microwave imaging is presented in Chapter 6. Emulation of stroke detection using TSVD microwave imaging algorithm is shown in Chapter 7. Chapter 8 concludes this white paper, underlying how one can benefit from the proposed 3D EM simulation environment.

2. Creation of head phantom model by using STL files of human body

In cooperation with NEVA (Bio) Electromagnetics [9], WIPL-D offers access to anatomically accurate human models of a man and a woman for electromagnetic simulations. The models differ in complexity, although both represent a complete human organism. These models consist of a large number of STL files that can be combined into a single STL project. Each file represents a closed structure corresponding to some type of tissue. These structures include organs, muscles, bones, nerves, blood vessels, skin, fat… A glimpse of one such, triangular based human model (in this case it is “Static VHP-Female model v2.2 of NEVA Electromagnetics”), with different tissues included in the project, is presented in the Figure 1.

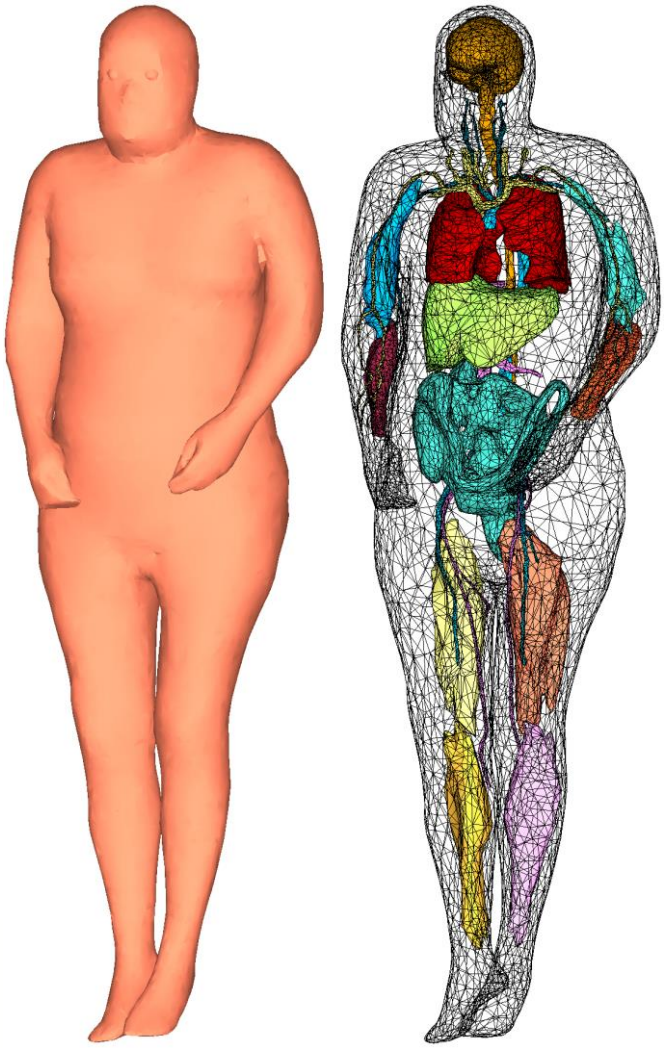

Figure 1. NEVA EM developed anatomical human model for electromagnetic simulations

Different EM simulations, intended for understanding, analysis or testing of medical devices, can be performed on these human models, or some of their parts. Stroke detection scenario, for example, requires only some of the tissues positioned inside the head. Combining only the tissues significant for a particular scenario into an STL project, not only simplifies the measurement setting, but also leads to a reduced number of unknowns. Reduced number of unknowns ensures faster simulation.

When designing a measurement scenario, the first step should be to choose the phantom and determine which of the tissues are required. For our stroke detection scenario, we opted for skin, fat, mucous membrane (as the basic head filling), brain and skull.

Some of those tissues are completely placed in the zone of interest (in this case it is the zone of the head), while others cover the whole body or a larger part of it. Skin and fat layers are the most basic examples of tissues that surround the entire body. There are two approaches to minimize such tissues:

1. Processing multiple tissues simultaneously. It implies importing all the tissues of interest and performing STL plane cropping operation that will affect all the tissues which results in multiple openings. Closure of the largest closed-loop hole/opening existing in the resulting model (in this particular case it is the skin layer opening) using **STL Fill** option, followed by **Complete Healing** option will create a well-connected and fully closed structure.

2. Systematic approach that involves special editing of different tissues. It usually includes importing one tissue at a time and performing different STL plane cropping and STL filling operations on separate tissues. Separation of tissues (distance between them) in the vicinity of the cropping area should also be considered within that location. Therefore, all individual tissues would remain closed and adequately separated.

This second approach not only leads to reduction of number of the triangles in the model (8362 for the second approach compared to 8866 using the first one), but it also eliminates the direct interaction between surrounding material (vacuum) and materials located inside the head phantom, leading to less computational time.

For our simulation setup, we opted to implement the second approach to phantom minimization/localization.

When certain STL file of non-WIPL-D origin (not saved or exported using WIPL-D Pro) is opened or imported in WIPL-D Pro for the first time, all triangular shaped plates in the model are recorded as metallic (PEC) structures positioned in air (i.e. (1, 0) for the domain definition) as there is no relevant data for material parameters.

After including all the required human tissues into the project and performing required geometrical modifications, we ended up with a completely metallic human head model. Next step is to include necessary domains parameters/definitions in the project and place them on appropriate plates/tissues. Prior to this, a user is advised to set the frequency range of interest (in our case it is the single frequency of 1 GHz). For this step, WIPL-D offers **Library of materials** that is included in the software. This advanced materials library is very useful for biomedical applications as it contains a substantial list of frequency dependent human tissue parameters.

Placing correct domain definitions on plates may appear to be difficult, but options such as **Select Layer** and **Hide Selected Plates** can significantly facilitate it. The Select Layer option invokes selection of connected plates limited by edges shared by more than two plates. Most times such selection corresponds to plates sharing the same domain specification. Hiding plate or groups of plates is especially important when working with multilayer structures, as it allows an access to the otherwise invisible parts of the structure. Results of two different head area modeling approaches, one that applied single crop and fill operation as well as healing of the structure that assured connectivity between tissues, and the other that required different modifications to be performed on several tissues, assuring the right distance between them is preserved, are presented in the Figure 2. Both models are presented after the domains were set.

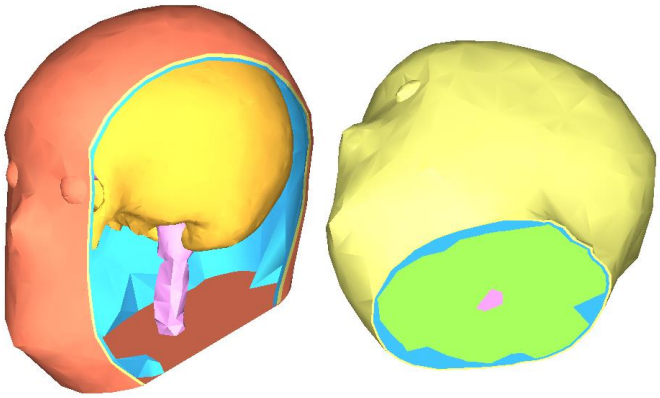

(a) Phantom resulting from single crop and fill operation approach that extracted head area

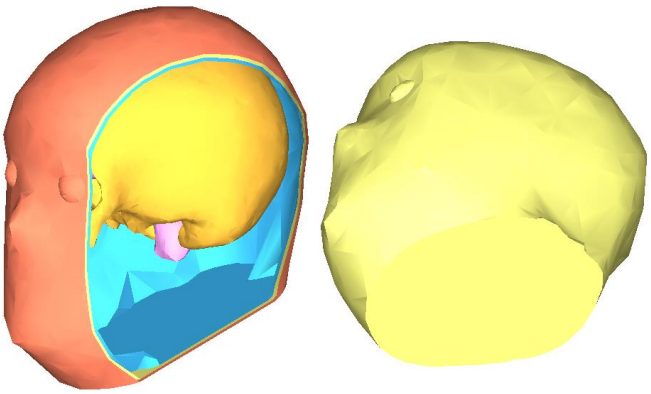

(b) Phantom resulting from methodical approach with multiple crops and fillings

Figure 2. Head phantoms after all adequate domain parameters were set to tissues

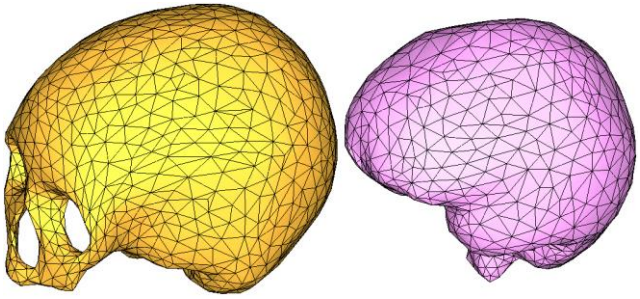

(a) STL models of skull and brain

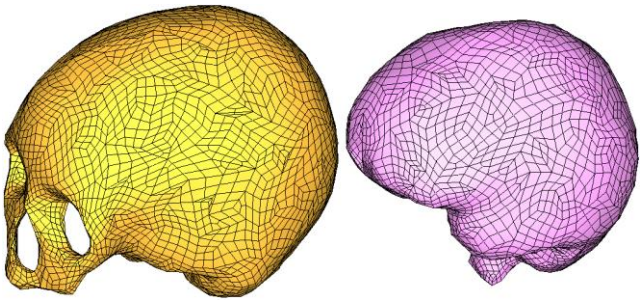

(b) WIPL-D model showcasing skull and brain tissues with no decimation included in procedure

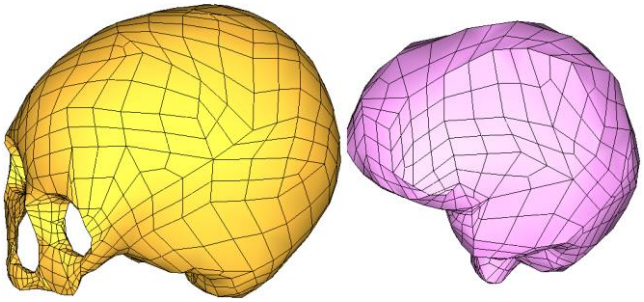

(c) WIPL-D model showcasing skull and brain tissues with maximum decimation of 3 mm included

Figure 3. Head Phantom

After completing the geometry and setting the domains, selection of scattering operation mode, defining plane wave excitation and specifying a grid of points for Near-Field calculation are performed next.

STL Decimation is the option intended for complex structures made of large number of triangles. It allows reducing the number of triangles in the structure while retaining the overall shape and size. This ensures that decimated model will be a good representation of the original. It is recommended to apply this option on multilayer structures since decimation algorithm avoids intersections. Decimation tool only requires the **Maximum allowed deviation** permitted for the output model as input parameter.

STL Meshing is the method to switch from triangular to quadrilateral mesh (STL file -> IWP file, IWP being a native WIPL-D format). Meshing can be performed on any STL model (starting one or one previously decimated).

If decimation is needed, we especially advise not to use it as a stand-alone option, but to apply meshing that has an integrated decimation. This option includes all the benefits of decimation, but at a same time it translates all the nodes produced by the meshing procedure to the original complex structure. This way we obtain a simplified, but geometrically extremely accurate representation of the structure.

Please note that both, meshing and decimation procedures, display the average deviation (RMS deviation) value calculated for the obtained model, as an output parameter. The value shows how much the resulting model differs from the initial one.

Our STL phantom is made of 8362 triangles. Meshing performed without decimation leads to a model that has 18664 plates/quadrilaterals. Allowing a maximum of 3 mm decimation leads to a model made of just 6850 plates. Even though we allowed maximum deviation to be 3 mm, the RMS of meshed model is just 0.506 mm from original triangular model. STL project together with IWP models obtained with no decimation or decimation of 3 mm is presented in the Figure 3.

3. Near-field for head phantom model excited by plane wave

We have already chosen operation mode, set plane wave excitation and selected grid of points to be used in Near-Field calculation, all while working on the STL project. Domain parameters were included in the STL project and domain settings were appointed to plates. All those settings propagated through meshing procedure resulting in a simulation ready WIPL-D project. Our goal was to calculate electric field inside the regular head, but also inside the one that includes the blood stroke. The stroke was modeled as a spherical object with a 15 mm radius. Near Field is set to be calculated in the vertical plane that includes center of the stroke. The **Selected near-field calculation** option enables that the field is calculated just inside the head. Another specialized WIPL-D tool allowed us to analyze obtained near-filed files for situation with and without the blood stroke and create a near-field result presenting the difference in the field for two situations (presence and absence of stroke). Three different results of electric field for plane wave excitation can be examined from Figure 4. Note that differential field is one to two orders of magnitude lower than total field with and without the stroke.

4. Adjusting antenna from library to head phantom model

In WIPL-D Pro software we also offer some of predefined antennas. All those antennas are defined symbolically (parametrically) and are frequency dependent. Antennas are set to work around 1 GHz, but the central frequency is adjustable. With the change of value for the symbol that defines central frequency the dimensions of the antenna change accordingly, providing a fairly good starting point for antenna solution.

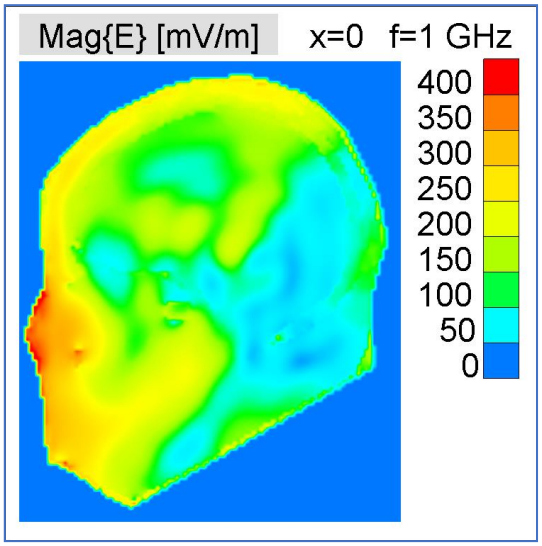

(a) Electric field results inside head without the stroke

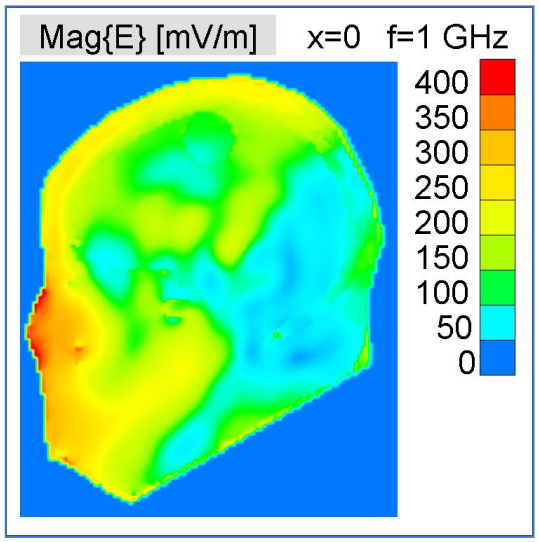

(b) Electric field results inside head with the stroke

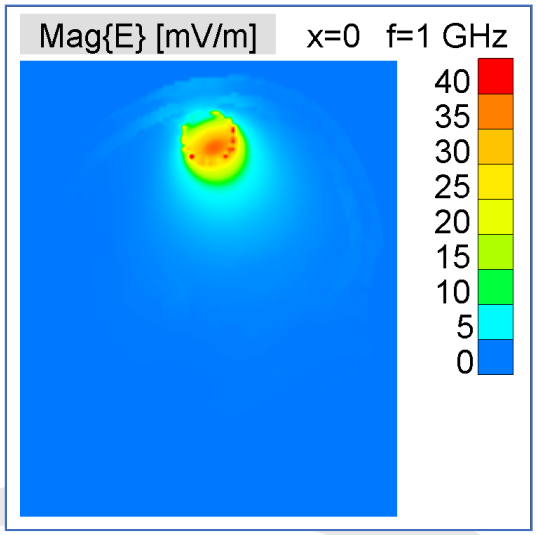

(c) Differential electric field value inside the head

Figure 4. Near-Field results (Electric field) inside the head

Several of these antennas can be used in biomedical applications. These Antennas customized for biomedical applications share the feeding area, which is the coaxial line. Also, antennas for medical applications possess a spacer made of matching media. The existence of the spacer reduces the field distortions in the space between antennas and the human tissues/organs, improving the communications between the antennas in array which leads to a better MWI results. Antennas adapted to MWI computation are:

- Microstrip Trapezoidal Patch (MTP) antenna
- Refined Microstrip Trapezoidal Patch (MTPR) antenna
- Pentagonal Arm Dipole (PAD) antenna
- Open waveguide (OWG) antenna

These four antennas can be seen in the Figure 5. In this work we use the MTPR antenna.

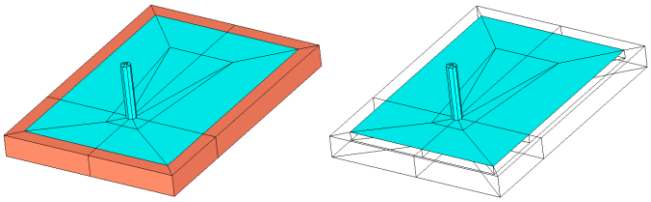

(a) Microstrip Trapezoidal antenna

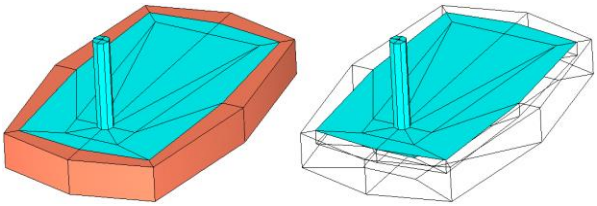

(b) Refined Microstrip Trapezoidal Patch antenna

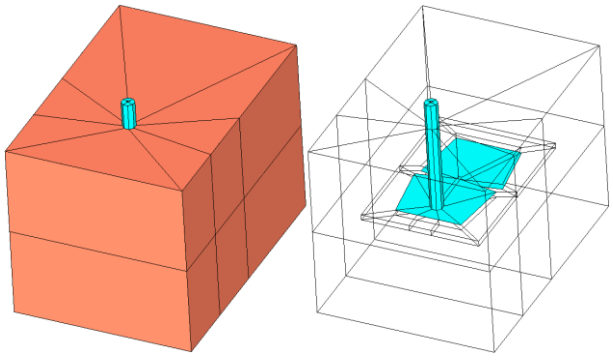

(c) Pentagonal Arm Dipole antenna

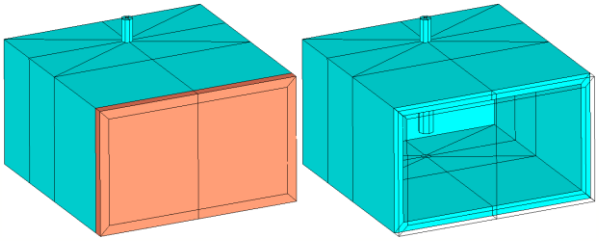

(d) Open Waveguide antenna

Figure 5. Antenna Library for medical applications

We have learned from the experience that, in order to provide good input parameters for the MWI algorithm, antennas used in the array should be well matched. The matching should be designed to be good for the antenna suspended in the air (vacuum), but also to remain good in the presence of the head model.
Basic model of an MTPR antenna was a nice starting point for us as it is already set to work around a central frequency of 1 GHz. S11 antenna parameters of regular MTPR antenna positioned in vacuum, calculated in the range from 0.8 GHz to 1.2 GHz, is displayed in the Figure 6.

In order to provide batter matching around 1 GHz, WIPL-D optimization tool was used. Values of several dimensional parameters have been varied during optimization. Optimization was performed at 5 frequency points: 0.9 GHz, 0.95 GHz, 1GHz, 1.05 GHz, and 1.1 GHz, with targeted values for S11 being less then: -15 dB, -15 dB, -20 dB, -15 dB, and -15 dB respectively. 75 iterations of particle swarm optimization method were used, followed by 275 iterations of simplex optimization technique.

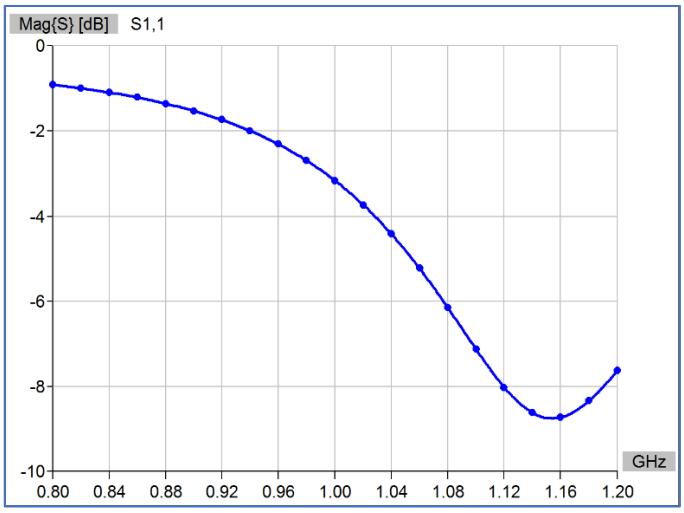

Figure 6. S11 parameters of regular MTPR antenna

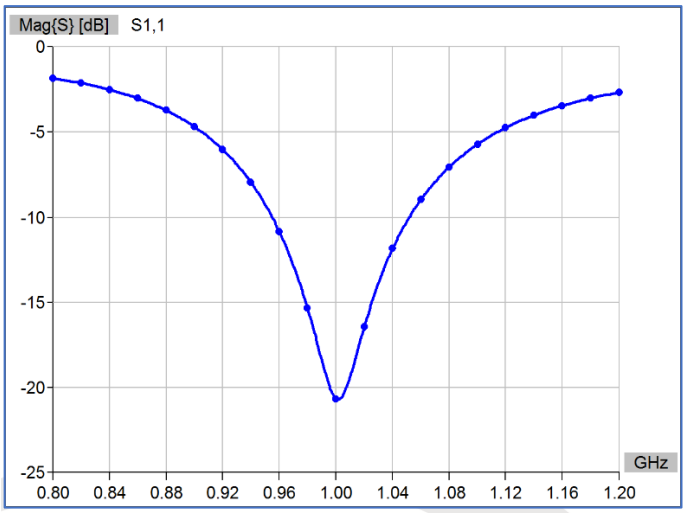

Figure 7. S11 parameters of optimized MTPR antenna

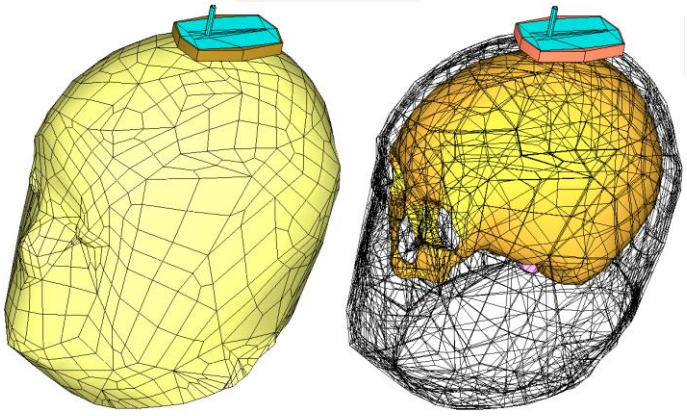

(a) Position of antenna in respect to the head model

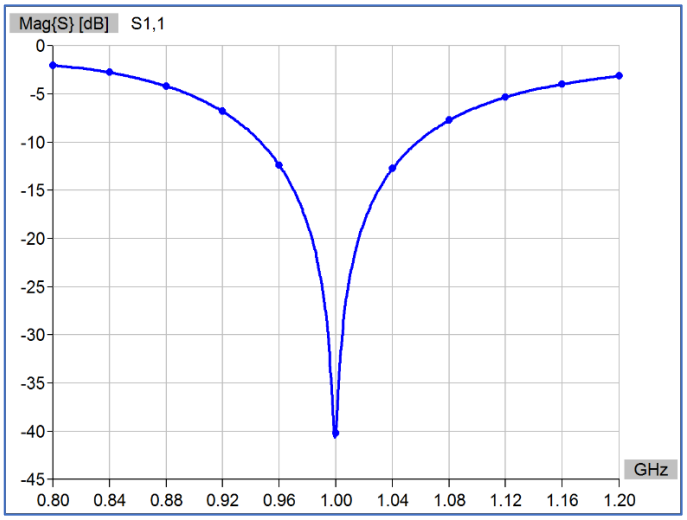

(b) S11 parameters

Figure 8. Optimized MTPR antenna placed near the head

The PC used for optimization is a desktop computer: Intel i7 920 CPU (2.67 GHz), 32 GB RAM. For optimization to complete, around two hours (7224 sec) were needed.

S11 antenna parameter of optimized MTPR antenna positioned in vacuum, in range from 0.8 GHz to 1.2 GHz, are presented in the Figure 7.

Before introducing optimized antennas into the setup, S11 parameter of antenna positioned close to a head should be calculated. If the matching is below -10 dB at frequencies of interest we can perform further steps necessary to create a helmet shaped antenna array. If not, additional optimization of antenna located in the close proximity to the head is required.

Optimized antenna in presence of the head, along with results for S11 is given in Figure 8. We conclude that the matching is more than satisfactory for microwave imaging purposes.

5. Semi-automatic design of antenna array helmet

The antenna systems in MWI scenario play key role for efficient and reliable simulations. Designed antenna array need to be as compact as possible, as close to the surface of the body as possible, and to cover the maximum surface around the area of interest. In order to design such system around the NEVA head, a semi-automatic procedure is developed. In the first step we determine the position and semi-axes of a half ellipsoid that approximates in the best way the part of the head that should be covered by antenna array, as shown in Figure 9. In addition, input data for design of antenna array helmet is rectangular or octagonal footprint of antenna that will be used as element of the array, as shown in Figure 10.

In the next step, 21 such octagon patterns are symmetrically placed around the half-ellipsoidal shape with the help of the semi-automatic algorithm. The algorithm firstly provides the arrangement of octagon patterns and then allows the patterns to closely pack around the head without intersections between the individual patterns. The number of antenna is set to 21, as this is the optimal maximum number of patterns that covers the entire surface of ellipsoidal shape. The algorithm also enables to closely attach the patterns to the head as shown in the Figure 11.

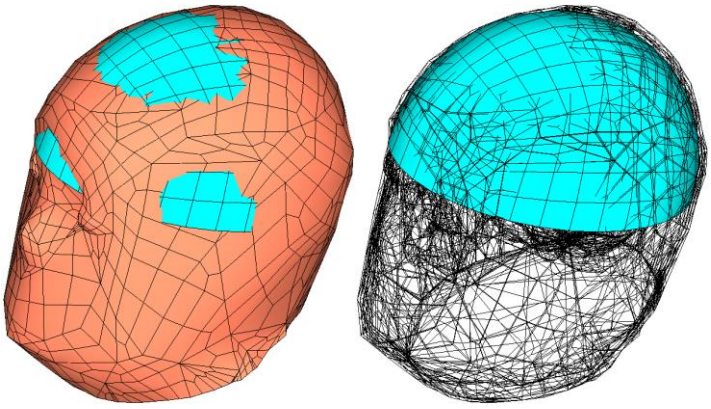

Figure 9. Upper half of the head comparable to half ellipsoidal shape

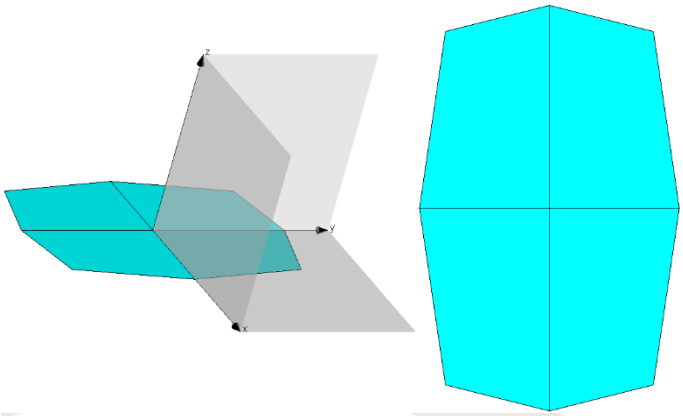

Figure 10. Octagon pattern similar to MTPR antenna structure

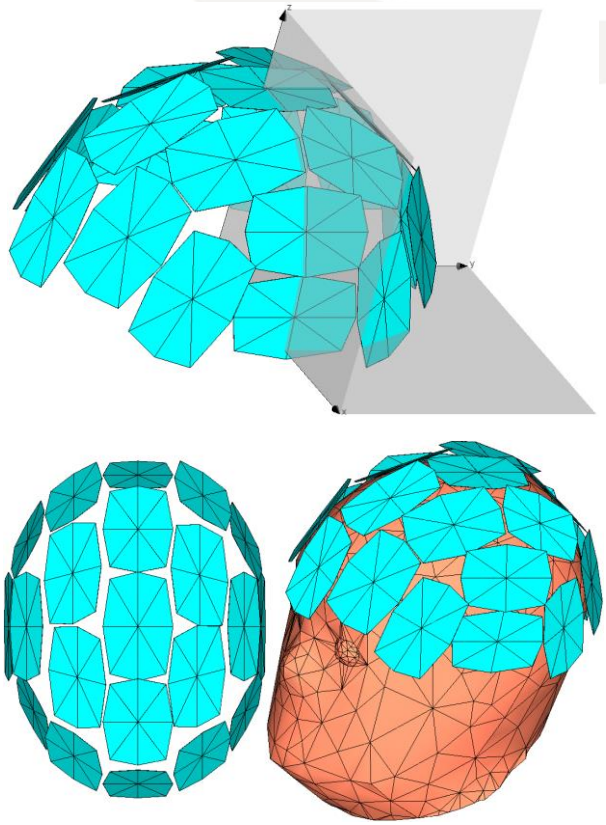

Figure 11. Semi-automatic helmet around the NEVA head

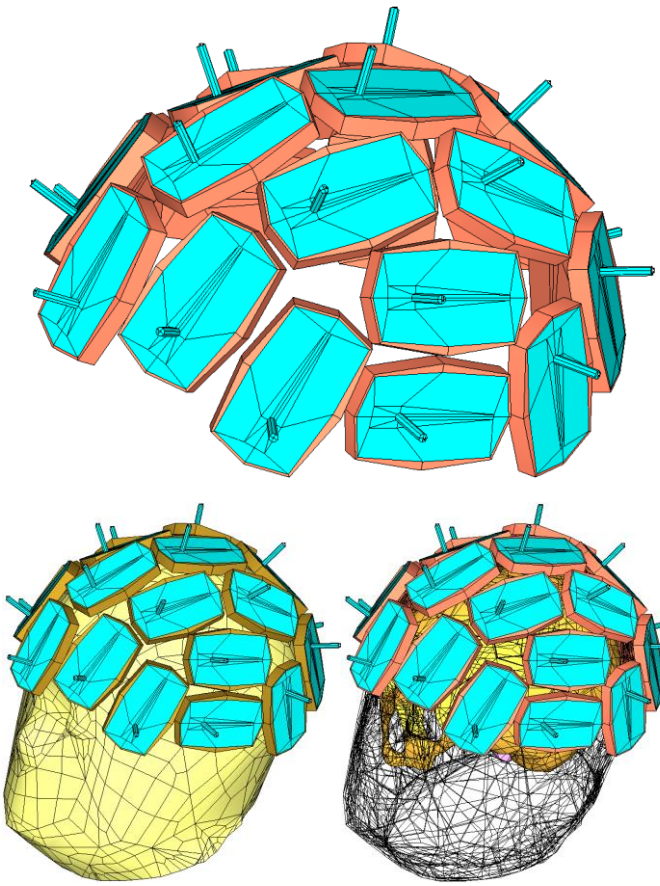

Figure 12. MTPR Semi-automatic Helmet placement around the NEVA head

The output of the algorithm is to provide the location of these patterns which can be further used in the WIPL-D Project to position antennas around the NEVA head with close packaging as shown in the Figure 12.

The Figure 12 represents densely packed antenna system covering maximum surface of upper half of the head, where the stroke possibly occurs.

6. Accuracy and usability of scenarios with/without stroke for MW imaging

Figure 4 clearly indicate that inclusion of stroke into the phantom model causes relatively small deviation of near field, i.e. differential field is one to two orders of magnitude lower than total field with and without the stroke. Similar results are valid for near field and s-parameters if the human phantom is excited by one by one antenna from the helmet.

Figure 13 shows s_{1j} - parameters versus j for the cases without and with the stroke, as well as their difference (differential s_{1j} - parameters, ds_{1j}). Difference between s-parameters in these two cases is so small that magnitude of differential parameters cannot be read visually from this graph having linear scale from 0 to 35 mU. Hence, the same differential parameters are also shown in Figure 14 in a linear scale from 0 to 180 μU. It is seen that magnitude of differential s-parameters is about 200 times lower than that of s-parameters. (Alternative presentation in logarithmic scale would show that level of differential parameters is below -70 dB.)

Given such small magnitudes of differential near field and s-parameters, the question arises as to how accurately the results should be calculated in order to be usable for emulation of stroke detection by microwave imaging. Note that most of qualitative and quantitative microwave imaging methods are based on calculation of S-operator, which represents the transfer function between change of electrical parameters of part of body and related differential s-parameters. Calculation of exact S-operator requires knowledge of both, incident and total, near field in the area of interest for the case when one by one antenna are excited, while other antennas are matched. However, if the changes of electric properties are relatively small, the incident field can be used instead of total field (Born approximation), resulting in an approximate form of S-operator. In that sense, we can consider that 3D EM simulation is sufficiently accurate and usable for emulation of stroke detection by microwave imaging if differential s-parameters calculated via exact and approximate S-operator are sufficiently close to those initially calculated via antenna ports.

Figure 14 shows three sets of differential s_{1j} - parameters versus j, calculated via 1) antenna ports, 2) exact S-operator, and 3) approximate S-operator. It also shows deviations of sets obtained via S-operator from that obtained via antenna ports.

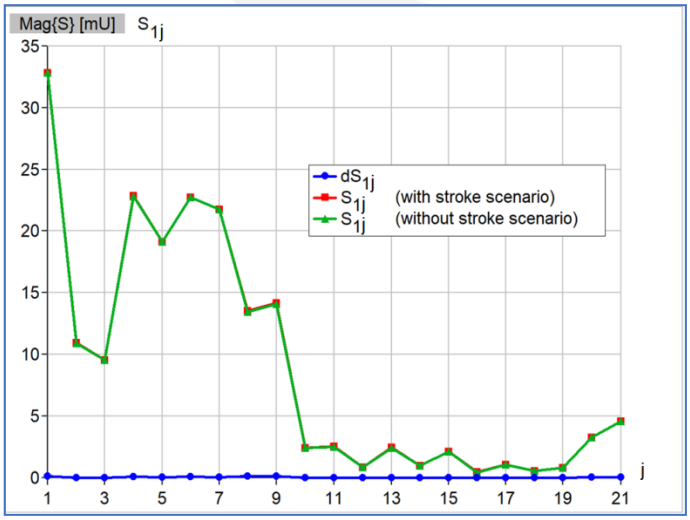

Figure 13. S-parameters as a function of port and also the difference of S-parameter between both scenarios.

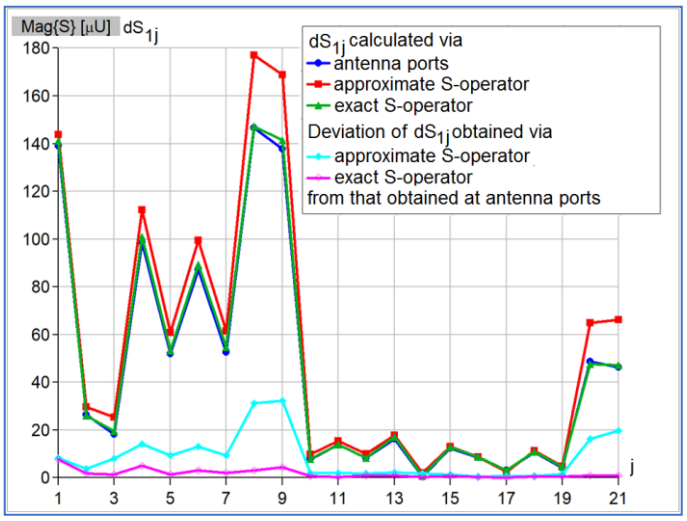

Figure 14. dS-parameters as a function of port for exact and approximate conditions.

It is seen that results for differential s-parameters obtained via exact S-operator almost coincide with those calculated at antenna ports, while those obtained via approximate S-operator are slightly different. Similar results are obtained for s_{ij} and ds_{ij} - parameters, for i=1,…,21.

Taking into account results for all values of indices i and j, relative RMS deviation is calculated for dS_{ij} - parameters obtained via S-operator with respect to those obtained via antenna port. In the case of exact variant of S-operator the relative RMS deviation is 2.88 %, while in the case of approximate S-operator this deviation is 20.6 %. It is concluded that deviation due to 3D EM simulation is negligible when compared to that due to Born approximation. It proves that proposed 3D EM simulation is sufficiently accurate and usable for emulation of stroke detection by microwave imaging.

7. Emulation of stroke detection using TSVD Microwave Imaging Algorithm

The 3D EM simulation is performed on proposed MWI scenario providing S parameter and near field data as .ad1 and .nf1 extension of WIPL-D native format. The data contains S-parameters for two scenarios, one with spherical stroke and one without stroke and near filed calculation in the observation domain (all domains contained inside the head) for the one without stroke. The grid of points for near field analysis is set for several horizontal cuts and one of the horizontal layer of grid in xOy plane coincides with center of spherical stroke. There are three input data for computational analysis of TSVD algorithm, a) .ad1 file with stroke, b) .ad1 file without stroke and, c) .nf1 file without stroke. The results are obtained in the form of pixelated image as shown in the Figure 15 where pixels are normalized to unity, for several horizontal cuts (parallel to xOy plane) including the one where center of stroke exits. The pixels with red color inside the reference boundary of actual spherical stroke, represented by a circle, gives impression of stroke as a contrast between healthy and damaged tissues.

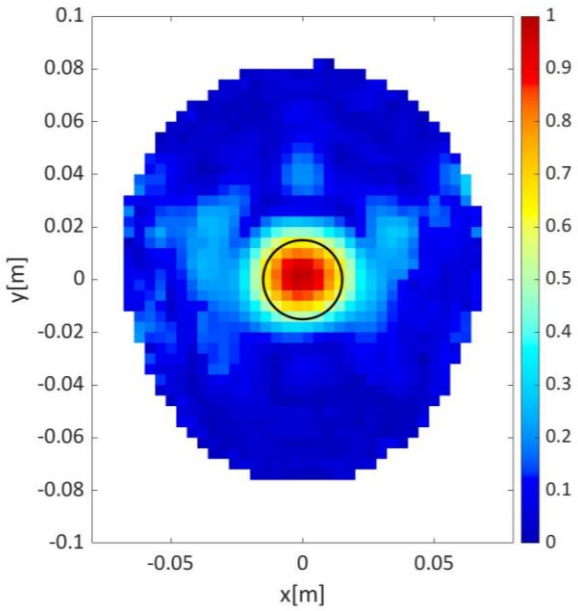

Figure 15. Microwave imaging result obtained from TSVD algorithm for one layer with center of stroke (0. 0. 62 mm)

8. Conclusion

We have come up with a fully functional module developed on WIPL-D Pro 3D EM simulation environment for Microwave Imaging applications. For such applications, the software provides flexibility in the use of STL files with the help of STL editor to develop anthropomorphic phantoms. It enables the user to analyze complexity of triangular mesh structures and allows to significantly reduce the computational requirement for the EM Simulation. For better accuracy and efficacy STL files with triangular mesh are converted to quadrilateral mesh. Further, to create the whole imaging scenario, an antenna system is developed with semi-automatic procedure. The automation system closely packages the antennas in the vicinity of the desired area of head, considering no intersection between the plates. The imaging scenario is simulated at 1 GHz frequency. To understand the efficiency and accuracy of EM simulation, differential S parameters are inspected through direct approach (simulation result) and also with the help of transfer function of TSVD microwave imaging algorithm. Subsequently, simulated data for two different scenarios with and without stroke is used as input to the TSVD algorithm to detect and estimate the size and location of stroke for brain stroke application.

References

[1] B. Kolundzija, M. Nikolic-Stevanovic, M. Stevanetic, B. Ninkovic and T. Singh, "Advanced 3D EM Simulation Environment for Development, Testing, and Usage of Medical Microwave Imaging Devices." 14th International Conference on Advanced Technologies, Systems and Services in Telecommunications 2019 (TELSIKS 2019), 23rd to 25th October, 2019.

[2] B.M. Kolundžija, A.R. Djordjević, „Electromagnetic modeling of composite metallic and dielectric structures", Boston: Artech House, 2002.

[3] WIPL-D software suite (WIPL-D Pro v17 & Pro CAD 2020), WIPL-D d.o.o, Belgrade, 2020.

[4] T. Singh, M. N. Stevanovic and B. Kolundzija, "Survey and Classification of Antennas for Medical Applications," 2019 13th European Conference on Antennas and Propagation (EuCAP), 2019, pp. 1-5.

[5] T. Singh, S. Abedi, B. Ninkovic, M. N. Stevanovic, N. Joachimowz, H. Roussel and B. Kolundzija, "Smart Simplification of Anthropomorphic Head Phantom Aimed for Microwave Imaging," 2021 15th European Conference on Antennas and Propagation (EuCAP), Düsseldorf, Germany, 2021, pp. 1-4.

[6] Hopfer, M.; Planas, R.; Hamidipour, A.; Henriksson, T.; Semenov, S. "Electromagnetic Tomography for Detection, Differentiation, and Monitoring of Brain Stroke: A Virtual Data and Human Head Phantom Study." IEEE Antennas Propag. Mag. 2017, 59, 86–97.

[7] J.A. Vasquez Tobon, R. Scapaticci, G. Turvani, G. Bellizzi, D. O. Rodriguez-Duarte, N. Joachimowicz, B. Duchêne, E. Tedeschi, M. R. Casu, L. Crocco, and F. Vipiana, "A Prototype Microwave System for 3D Brain Stroke Imaging," Sensors 2020, 20, 2607.

[8] J. Shea, B. Van Veen, S. Hagness, "A TSVD analysis of microwave inverse scattering for breast imaging," IEEE Transactions on Biomedical Engineering, vol. 59, no. 4, pp. 936–945, 2012.

[9] https://www.nevaelectromagnetics.com/